Appl. Phys. A 62, 503–508 (1996)

Applied Physics A Materials Science & Processing

Pyrolytic LCVD of fibers: A theoretical description

N. Arnold*, E. Thor, N. Kirichenko, D. Bäuerle**

Angewandte Physik, Johannes-Kepler-Universität, Linz, A-4040, Linz, Austria
(Fax: + 43-732/2468-9242, E-mail: NIKITA.ARNOLD@jk.uni-linz.ac.at)

Received: 1 February 1996/Accepted: 5 February 1996

Abstract. The pyrolytic LCVD (Laser-induced Chemical Vapor Deposition) of fibers is studied theoretically. The shape of fibers and the temperature distribution are calculated self-consistently on the basis of a one-dimensional model which takes into account changes of the radius along the fiber. The influence of different parameters on the fiber radius and the temperature is discussed. The parameters investigated include the laser power and spot size, the activation energy of the deposition reaction, diffusion limitations in the gas phase, and temperature dependences of the heat conductivities of the deposit and the gas. The results are applied to the pyrolytic growth of Si fibers from $SiH_4 + H_2$.

PACS: 81.15.Gh; 44.10. + i; 42.55. − f; 68.55.Gi

During the last decade, pyrolytic laser-induced chemical vapor deposition (LCVD) [1, 2], has attracted attention as a convenient tool for repair and customization of electronic devices, and for the production of micromechanical devices and different types of sensors [3]. In pyrolytic LCVD, deposition proceeds in the area locally heated by the laser beam.

Early studies concerned deposition of spots, fibers [4, 5], and lines (laser direct writing) [6, 7]. The geometrical parameters of lines were studied experimentally and theoretically [8–10].

Under certain conditions, fibers may start to grow towards the laser beam [11, 12] and three-dimensional objects can be fabricated in this way [13, 14]. The purpose of this article is to describe theoretically the shape of fibers and their dependence on experimental parameters and material properties.

* To whom correspondence should be addressed
** *On leave from: General Physics Institute, Academy of Sciences, 117942 Moscow, Russia*

1 Model

A schematic picture of the growth process is presented in Fig. 1. The laser beam is focused at the tip of the fiber. Pyrolytic decomposition of gas-phase precursors proceeds in the hot area near the tip due to the strong dependence of the reaction rate, W, on temperature, T. Changes in the fiber radius take place mainly in this region. Due to the big difference in thermal conductivities of the deposit and gas, $\kappa_d \gg \kappa_g$, the heat flows along the deposit and then gradually dissipates into the surrounding gas. For long fibers, the influence of the substrate becomes unimportant and their radius and shape become dependent only on the absorbed laser power P, the radius of the laser focus w_0, the properties of the gas and the deposit, and the parameters that characterize the pyrolytic decomposition reaction.

With the experimental conditions employed in LCVD, the propagation of heat is much faster than typical growth rates, i.e., $D_T/l \gg W$ ($D_T \approx 0.1$–$1\ \mathrm{cm}^2/\mathrm{s}$ is the heat diffusivity, $l \approx 10$–$100\ \mu\mathrm{m}$ is the characteristic distance (1.7)). Correspondingly, we consider the stationary heat equation for the fiber, taking into account changes in the radius $R = R(z)$, and heat losses into the ambient medium (second term in (1.1a)):

$$\frac{\partial}{\partial z}\left(\pi R^2 \kappa_d \frac{\partial T_d}{\partial z}\right) + 2\pi R \kappa_g \left.\frac{\partial T_g}{\partial z}\right|_{r=R} = 0, \tag{1.1a}$$

$$-\left(\pi R^2 \kappa_d \frac{\partial T_d}{\partial z}\right)\Bigg|_{z=0} = AP, \tag{1.1b}$$

$$T_d|_{z=\infty} = T_0. \tag{1.1c}$$

Here, κ_d and κ_g depend on the temperature of the deposit, T_d, and the gas, T_g, respectively. A is the absorptivity and T_0 the ambient temperature. Because of the small temperature gradients within the deposit in radial direction, the temperature is assumed to depend on z only:

$$-\kappa_d \left.\frac{\partial T_d}{\partial r}\right|_{r=R} = -\kappa_g \left.\frac{\partial T_g}{\partial r}\right|_{r=R} \sim \kappa_g \frac{T_g(r=R)}{R} \sim \kappa_g \frac{T_d}{R} \tag{1.2}$$

$$\Rightarrow \frac{T_d(r=0) - T_d(r=R)}{T_d} \sim \frac{\kappa_g}{\kappa_d} \ll 1.$$

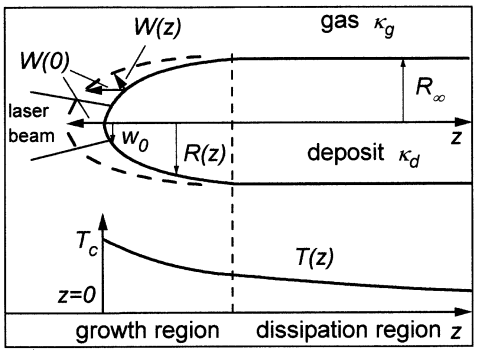

Fig. 1. Schematic picture of the 1D model. The shape of the deposit is given by $R = R(z)$ and the temperature distribution by $T(z)$. $W(z)$ is the growth rate at a particular point. Dashed curve near the tip of the fiber illustrates the growth process in the steady-state regime. In the dissipation region $T(z) \to T_0$, and $R(z) \approx R_\infty = \text{const}$

The heat equation (1.1) should be solved together with the equation of growth. At each point, characterized by the coordinates $(z, R(z))$, the deposit grows in the direction normal to the surface (Fig. 1). With *quasi-stationary* conditions we can write

$$\frac{\mathrm{d}R}{\mathrm{d}z} = \frac{W(z)}{W(0)}\left[1 + \left(\frac{\mathrm{d}R}{\mathrm{d}z}\right)^2\right]^{1/2} \Rightarrow \frac{\mathrm{d}R}{\mathrm{d}z} = \left[\left(\frac{W(0)}{W(z)}\right)^2 - 1\right]^{-1/2}, \tag{1.3a}$$

$$R|_{z=0} = \chi w_0. \tag{1.3b}$$

Here, $W(0)$ is the growth rate at the tip of the fiber at $z = 0$, and (1.3b) the initial condition for the radius $R(z)$, where, in the simplest case, $\chi \approx 1$.

If the dependence $W(z)$ is known, (1.1) and (1.3) allow to calculate self-consistently the steady-state radius of the fiber, $R_\infty \equiv R(z = \infty)$, and the temperature at the tip, $T_c \equiv T_d(z = 0)$.

In order to exclude temperature dependences in thermal conductivities from (1.1), we introduce linearized temperatures via the Kirchhoff transform [15]:

$$\theta(T) = \frac{1}{\kappa_0}\int_{T_0}^{T} \kappa(T)\,\mathrm{d}T, \quad \kappa_0 \equiv \kappa(T_0). \tag{1.4}$$

Within the gas, θ obeys the Laplace equation and we approximate the second term in (2.1a) by $-\kappa_g \partial T_g/\partial r(r = R) \approx \eta\kappa_{g0}\theta_g(z)/R(z)$. Here, the dimensionless coefficient is $\eta = 1$ with spherical geometry, and $\eta < 1$ with the present case, which is more close to a cylindrical problem. The estimation of η is given in the appendix.

The continuity of the temperature (we neglect any temperature jump) at the gas–deposit interface yields the relationship between the linearized temperatures:

$$T(\theta_d) = T(\theta_g) \Rightarrow \theta_g = \theta_g(\theta_d). \tag{1.5}$$

This can be calculated from (1.4), which should be written for the gas and deposit. This allows to rewrite (1.1) in the form

$$\frac{\partial}{\partial z}\left(l^2 \frac{\partial \theta_d}{\partial z}\right) - \theta_g(\theta_d) = 0, \tag{1.6a}$$

$$\left(R^2 \frac{\partial \theta_g}{\partial z}\right)\bigg|_{z=0} = -\frac{AP}{\pi\kappa_{d0}}, \tag{1.6b}$$

$$\theta_d|_{z=\infty} = 0, \tag{1.6c}$$

with the notation

$$l^2(z) \equiv \frac{\kappa_{d0}}{\kappa_{g0}}\frac{R^2(z)}{2\eta} \gg R^2(z), \tag{1.7}$$

l characterizes the typical scale of the temperature drop in z-direction.

Henceforth, we assume a one-step pyrolytic reaction. In the kinetically controlled region we assume an Arrhenius dependence:

$$W(z) \equiv W(T(z)) = W_0 \exp(-T_a/T), \tag{1.8a}$$

where T_a is the activation temperature and W_0 the preexponential factor. With high reaction rates, diffusion limitations within the gas become important and W can be approximated by the Smoluchowski equation [16]:

$$W = \frac{W(T)}{1 + \dfrac{\rho_d}{\rho_g}\dfrac{W(T)R}{D}} = \frac{W(T)}{1 + \dfrac{W(T)}{W_0}\dfrac{R}{R_{dif}}}, \qquad R_{dif} \equiv \frac{\rho_g}{\rho_d}\frac{D}{W_0}. \tag{1.8b}$$

Here, ρ_d and ρ_g is the density *of the deposited species* in the solid and the gas phase, respectively. D is the gas-phase diffusion coefficient, and W is given by (1.8a). Temperature dependences of W_0 and R_{dif} in (1.8b) are ignored, because they are weak in comparison to the exponent in $W(T)$.

Equations (1.3) and (1.6) should be solved together with (1.4), (1.5), and (1.8).

2 Analytical consideration

If diffusion limitations are ignored, approximate analytical solutions can be obtained. In this case, there exist two distinct regions along the fiber: the region where the radius changes due to growth and where the temperature does not decrease significantly, and the "dissipation" region where the radius of the fiber is almost constant. In this region heat losses to the ambient gas dominate, and the temperature decreases up to T_0. We write an approximate solution for both regions and combine them at the distance z, where $R(z) \approx R_\infty$ (Fig. 1).

In the region where R changes, we neglect the second term in (1.6a). That means that changes in the heat flux along the fiber are mainly due to changes in its cross-section, and not due to the losses into the ambient gas. Together with (1.7) and (1.6b), we obtain

$$R^2 \frac{\partial \theta_d}{\partial z} = \text{const.} = \left(R^2 \frac{\partial \theta_d}{\partial z}\right)\bigg|_{z=0} = -\frac{AP}{\pi\kappa_{d0}}, \tag{2.1}$$

It is possible to refine (2.1) by expanding the second term in (1.6a) into a Taylor series near $z = 0$. A comparison with numerical results in Sect. 3 shows that this does not lead to significant improvements in results.

In the growth region, $R(z)$ changes according to (1.3a). Dividing (1.3a) by (2.1) and using (1.4), we obtain

$$\frac{AP}{\pi} d\left(\frac{1}{R}\right) = \kappa_d(T)\left[\left(\frac{W(0)}{W(z)}\right)^2 - 1\right]^{-1/2} dT. \tag{2.2}$$

In the absence of transport limitations, W depends only on T and not on R, the variables are separated, and (2.2) can be directly integrated. The limits of integration are given by the physical meaning of the growth region: For the left-hand side of (2.2) they are $R(z=0)$ and R_∞. The main contribution on the integral at the right-hand side comes from the region near $z=0$, where $T=T_c$, and the right-hand side is singular. This allows to expand an exponential function on the right-hand side in a Taylor series near $T=T_c$ and use the saddle-point method [17]. Comparison with direct numerical integration of (2.2) shows that this procedure leads to an error of several percent. With $R(z=0)=\chi w_0$ integration yields

$$\frac{AP}{\pi}\left(\frac{1}{\chi w_0} - \frac{1}{R_\infty}\right) \approx \kappa_d(T_c) \int_{-\infty}^{T_c} \left[\exp\left(\frac{2T_a(T_c - T)}{T_c^2}\right) - 1\right]^{-1/2} \times dT = \kappa_d(T_c)\frac{T_c^2}{T_a}\frac{\pi}{2}. \tag{2.3}$$

The lower limit of integration can be set to $-\infty$ because $T_a/T_c \gg 1$.

Equation (2.3) relates the unknown quantities T_c and R_∞. The second relation is found from the solution of (1.6a) in the region (Fig. 1) where $R \equiv R_\infty = \text{const.}$, and $l^2 = l_\infty^2 = \text{const.}$, (1.7). In this case, (1.6a) is similar to an equation of motion in a potential field and possess an "energy" conservation law:

$$\frac{l_\infty^2}{2}\left(\frac{\partial\theta_d}{\partial z}\right)^2 - g(\theta_d) = \text{const.} \equiv 0, \qquad g(\theta_d) \equiv \int_0^{\theta_d} \theta_g(\theta_d')\, d\theta_d'. \tag{2.4}$$

The constant in (2.4) is equal to zero because the left-hand side vanishes with $z \to \infty$. We employ (2.4) at the boundary between the growth region and the dissipation region, where we assume that $R = R_\infty$, $\theta_d \approx \theta_d(T_c)$. The last statement means that the temperature does not change significantly throughout the growth region. The value of $\partial\theta_d/\partial z$ should be taken from (2.1) with l_∞^2 from (1.7). Rewriting the g function from (2.4) in terms of temperature, we thus obtain

$$\frac{1}{2\eta}\left(\frac{AP}{\pi R_\infty}\right)^2 = \int_{T_0}^{T_c} \kappa_d(T) \int_{T_0}^{T} \kappa_g(T')\, dT'\, dT \equiv I(T_c). \tag{2.5}$$

This equation, together with (2.3), allows to find T_c and R_∞ for temperature-dependent heat conductivities. Eliminating R_∞ from (2.3) we get the transcendental equation for T_c:

$$\frac{AP}{\pi\chi w_0} = \sqrt{2\eta I(T_c)} + \kappa_d(T_c)\frac{T_c^2}{T_a}\frac{\pi}{2}, \tag{2.6a}$$

$$R_\infty = \frac{AP}{\pi\sqrt{2\eta I(T_c)}}. \tag{2.6b}$$

In the general case, these equations can be easily solved numerically. In some cases, I in (2.5) can be calculated analytically. As an example, we consider constant heat conductivities κ_d, κ_g. Then,

$$I(T_c) = \kappa_d\kappa_g\frac{(T_c - T_0)^2}{2}. \tag{2.7}$$

If $T_c \gg T_0$, we obtain for T_c a quadratic equation with the solution:

$$T_c \approx \frac{T_a}{\pi}\left(\eta\frac{\kappa_g}{\kappa_d}\right)^{1/2}\left[\left(1 + \frac{2A}{\chi\eta}\frac{P}{w_0\kappa_g T_a}\right)^{1/2} - 1\right] \approx \left(\frac{2A}{\pi^2\chi}\frac{PT_a}{\kappa_d w_0}\right)^{1/2}. \tag{2.8a}$$

The latter approximation refers to cases where the second term in the square root is $\gg 1$, as it is usually the case in LCVD experiments. In this region,

$$R_\infty \approx \left(\frac{\chi A}{2\eta}\frac{Pw_0}{\kappa_g T_a}\right)^{1/2}. \tag{2.8b}$$

Expressions (2.8) give the general trends for the dependence of T_c and R_∞ on experimental parameters and material properties. More refined dependences may be obtained from (2.6) or, especially when transport limitations are involved, from numerical solutions of (1.3), (1.6) with (1.8).

3 Numerical considerations

The numerical procedure is organized as follows: The differential equations (1.3a) and (1.6a) are solved together. The Cauchy problem starting at $z=0$ requires 3 initial conditions which are given by (1.3b), (1.6b), and $T(z=0)=T_c$. all of them containing T_c which is yet unknown. The solution of the Cauchy problem allows to calculate the temperature far away from the tip of the fiber, $T_\infty(T_c)$, as a function of T_c. Then, the requirement $T_\infty(T_c) = T_0$ allows to find T_c by iterations. In the absence of transport limitations and for weak dependences $\kappa_d(T)$ and $\kappa_g(T)$, the analytical results (Sect. 2) coincide with the numerical results within 10–15%.

4 The influence of different parameters

In this section we discuss the influence of the laser power, laser spot size, the heat conductivities, and possible transport limitations, on T_c and R_∞. It is convenient to introduce the normalized radius $R_\infty/\chi w_0$ and the normalized temperature T_c/T_0. Then, we find their dependences on normalized power $PA/\pi\chi\eta\kappa w_0 T_0$, activation energy T_a/T_0, and heat conductivity ratio, $\kappa^* = \kappa_{d0}/\kappa_{g0}$.

4.1 Laser power

An increase in laser power always leads to an increase in T_c and R_∞, as it can be seen from Figs. 2–6. Usually, the dependence is between square root and linear with the

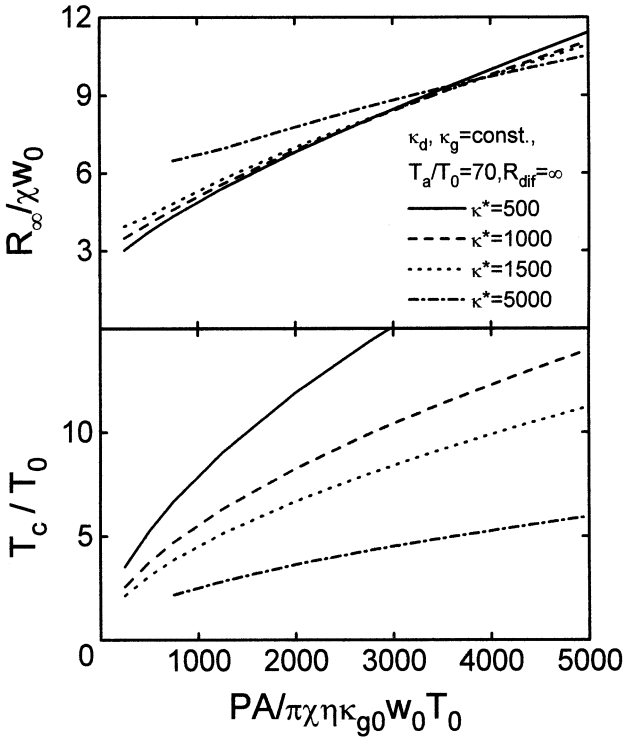

Fig. 2. Dependence of normalized radius and normalized temperature on normalized laser power in the kinetically controlled regime with $\kappa^* = \kappa_{d0}/\kappa_{g0}$ and $\kappa = 1$

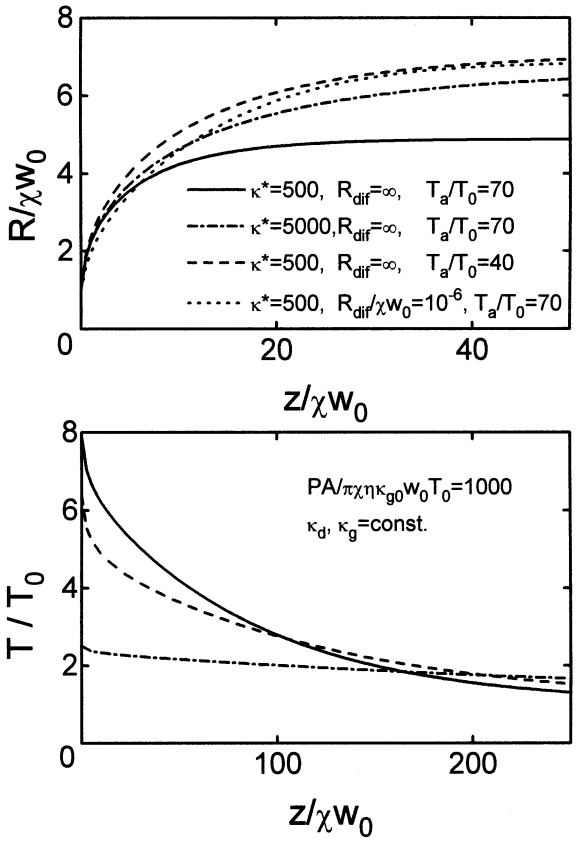

Fig. 3. Changes in radius and temperature distribution along the fiber for fixed laser power $PA/\pi\chi\eta\kappa_{g0}w_0T_0 = 1000$ and different thermal conductivity ratios κ^*, activation energies T_a, and R_{dif}. Dotted curve on the lower plot coincides with the dashed one

temperature increasing much slower than the radius. This is in agreement with experimental observations.

4.2 Laser spot size

T_c decreases and R_∞ increases with increasing w_0, as it can be seen from the simplified expressions (2.8). The decrease in T_c is due to smaller intensity near the tip of the fiber. When the normalized dependence $R_\infty(P)$ becomes close to linear, R_∞ becomes less dependent on w_0, as both normalized radius and normalized power are inversely proportional to w_0.

4.3 Ambient temperature

With the assumption $T_c \gg T_0$, T_0 does not enter the expressions for T_c or R_∞. Numerical calculations show that usually there exists a weak increase in both T_c and R_∞ with T_0 because it is easier to achieve higher temperatures with the same laser power.

4.4 Activation temperature (energy)

In agreement with (2.8), numerical results show that T_c increases with T_a while R_∞ decreases (e.g., Fig. 3, solid and dashed lines). With higher T_a, the effective growth region becomes shorter (more steep $W(T)$ dependence), and thereby R_∞ decreases. Thus, T_c increases due to the smaller heat flux along the fiber. The *preexponential* factor W_0 in the Arrhenius law influences neither T_c nor R_∞ because only *relative* changes in the reaction rate are important (1.3a)). Having in mind that for an ideal gas, κ_g is independent of pressure, this is in agreement with the experimental findings [18, 19] that $R_\infty(P)$ is almost independent of the pressure of the precursor and/or buffer gas.

4.5 Thermal conductivities

The dependence of T_c and R_∞ on κ_d and κ_g, respectively, is illustrated by Fig. 2. It is in agreement with approximation (2.8). T_c increases with decreasing κ_d due to the diminished heat flux along the fiber. With low powers P, R_∞ increases with κ^*. This is because with lower T_c, the region where $W(0)$ and $W(z)$ are comparable increases. (Fig. 3, solid and dashed–dotted curves).

The temperature-dependent heat conductivities have been described by n_d, n_g:

$$\kappa_d(T) = \kappa_{d0}(T/T_0)^{n_d}, \qquad \kappa_g(T) = \kappa_{g0}(T/T_0)^{n_g}. \tag{4.1}$$

Below we present numerical results (Sect. 3) which usually agree within 10–15% with analytical predictions (2.6). With $|n_{d,g}| > 1$, the agreement between analytical and numerical calculations becomes worse.

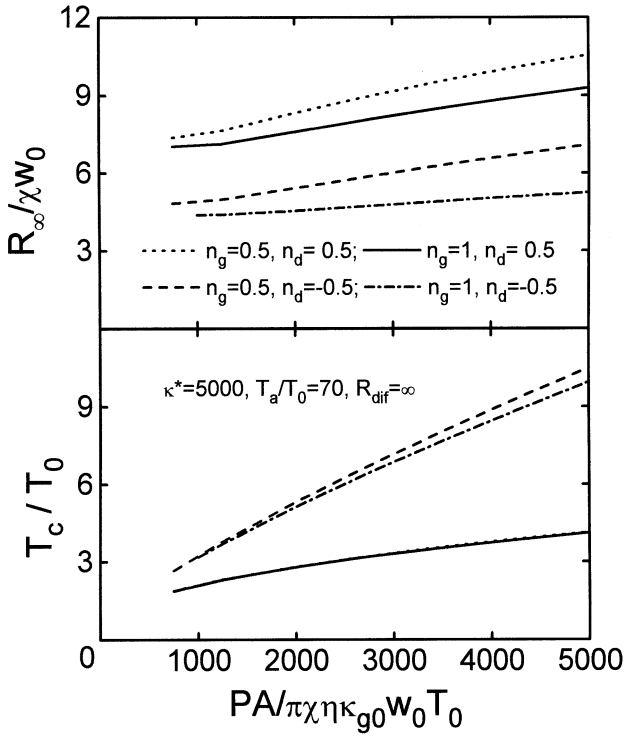

Fig. 4. Influence of temperature-dependent thermal conductivities (characterized by exponents n_d, n_g in (4.1)) on the radius and tip temperature

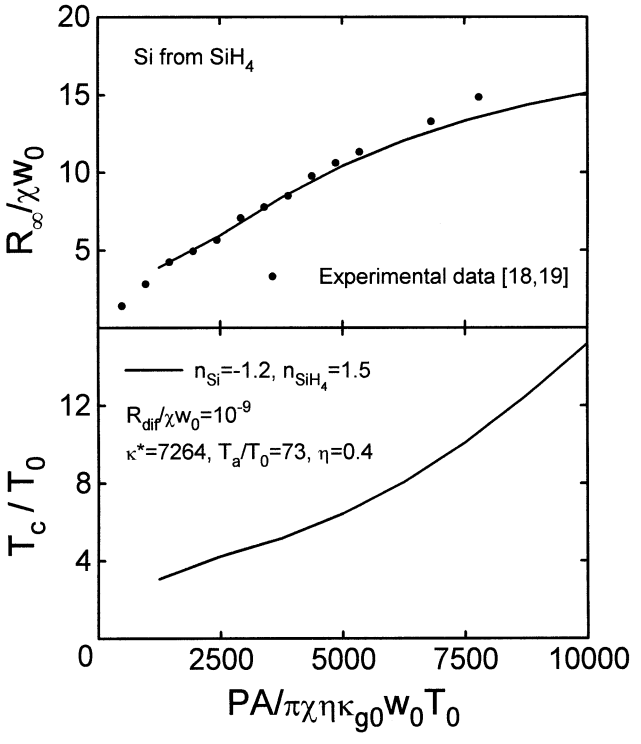

Fig. 6. Modeling of pyrolytic growth of Si fibers from SiH_4 [18, 19]. The values of parameters employed are $\kappa_g = 2.12\times10^{-4}\times(T/300)^{1.5}$ W/cm K, $\kappa_d = 1.54\times(T/300)^{-1.2}$ W/cm K [21], $A = 0.55$, $W_0 = 8780$ cm/s [18, 19], $\chi = 1$, $\eta = 0.4$

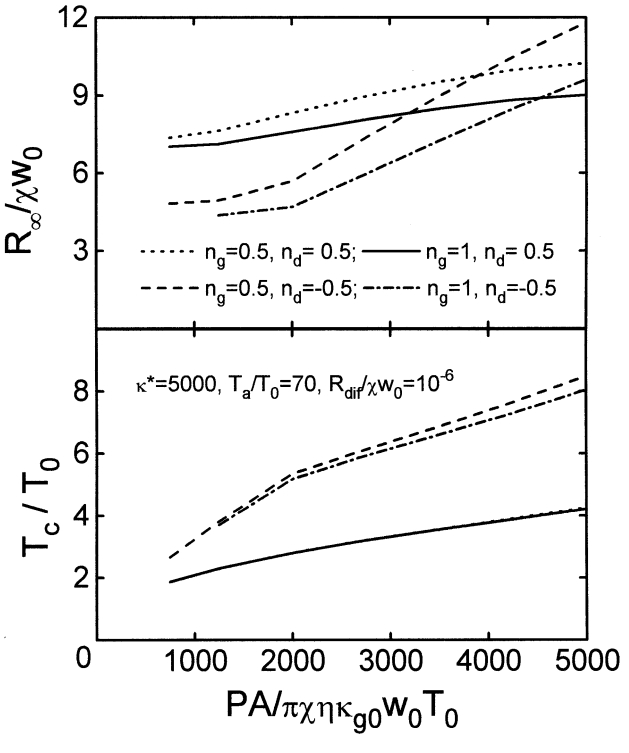

Fig. 5. Same as Fig. 4, but with finite diffusion, characterized by $R_{dif}/\chi w_0 = 10^{-6}$. At high laser powers transport limitations play an important role. T_c decreases while R_∞ increases with respect to the results in Fig. 4

T_c is mainly influenced by n_d, and R_∞ by n_g, as expected from (2.8) (Fig. 4). An increase in n_g increases the heat losses to the ambient gas, and thereby makes the temperature distribution sharper, which diminishes R_∞.

4.6 Transport limitations

Transport limitations in the gas phase, as described by (1.8b) significantly change the dependences $T_c(P)$ and $R_\infty(P)$ because they diminish *relative* changes of the reaction rate along the fiber. Correspondingly, the growth region becomes longer and R_∞ increases while T_c decreases. The effect of transport limitations is similar to that of a decrease in activation energy (Fig. 3, dotted and dashed curves). With temperature-dependent heat conductivities, the influence of diffusion may become particularly pronounced (Fig. 5). The transport limitations start when the denominator in (1.8b) is close to two at $T = T_c$ (Fig. 4). Thus, they occur at higher powers for higher values of κ_d, κ_g, n_d, n_g (bigger heat losses) and T_a (smaller reaction rate).

4.7 Ambient gas pressure

Without transport limitations, the gas pressure influences T_c and R_∞ only via κ_g. Corresponding changes may be estimated from (2.6) and/or (2.8).

If transport limitations become effective, the gas pressure enters R_{dif} in (1.8b) via ρ_g, D, and W_0. In the absence of a buffer gas this leads to $R_{dif} \propto 1/p$, which slightly shifts the transport limited region to a smaller P with increasing p.

5 Growth of Si from $SiH_4 + H_2$

We shall apply our model to the description of the pyrolytic growth of Si fibers from SiH_4 [4, 18, 19]. The parameters employed in the calculations are included in Fig. 6. Changes in laser power from 50 to 800 mW were considered. The fit is satisfactory, in particular, in the range of medium laser powers. With very low powers, when R_∞ becomes comparable with w_0, the assumption of a 1D geometry near the tip of the fiber becomes violated, and the model does not work satisfactory. With high powers it produces too small values of R_∞ and, correspondingly, too high T_c. This may be related to the fact that real values of material parameters at elevated temperatures may differ from those used in the calculations. For example, the deposit may contain a fraction of polycrystalline material with higher thermal conductivity which will effectively increases κ_d. A fit of comparable quality and better agreement at high laser powers may be obtained with $n_d = -0.8$ and $R_{dif}/\chi w_0 = 1.4 \times 10^{-8}$. No data are available for the diffusion coefficient of silane; the value of ρ_g which should be used in (1.8b) is somewhat arbitrary due to its temperature dependence, and the shape of the tip of the fiber differs from spherical which has been assumed in (1.8b). Correspondingly, R_{dif} was considered as a fitting parameter which varies within a physically admissible range.

6 Conclusions

The one-dimensional model investigated allows us to understand many features observed experimentally during pyrolytic growth of fibers by laser CVD. The dependences of the fiber radius and the stationary temperature in the reaction zone on laser power, spot size, activation temperature, and heat conductivities are studied. The influence of gas-phase transport is discussed as well.

Simplified analytical formulas are presented together with numerical calculations. The results have been applied to the pyrolytic growth of Si fibers from SiH_4.

Acknowledgements. We wish to thank Prof. B. Luk'yanchuk for valuable discussions and the "Fonds zur Förderung der Wissenschaftlichen Forschung in Österreich" for financial support.

Appendix

The heat exchange coefficient η

Far away from the tip of the fiber the temperature distribution within the gas is spherical and is given by

$$\theta_g = AP/4\pi\kappa_{g0}. \tag{A1}$$

The temperature along the fiber in the region where its radius remains constant is given by (2.4) which, in the case of constant heat conductivities (2.7), degenerates into

$$\theta_g \equiv \theta_d = \theta_c \exp\left(-\frac{z}{l_\infty}\right) \approx \frac{AP}{\pi 2\eta l_\infty \kappa_{g0}} \exp\left(-\frac{z}{l_\infty}\right). \tag{A2}$$

The last equality follows from the energy conservation in the dissipation region and (1.7).

At a distance $r \approx z \approx l_\infty$, (A1) and (A2) should coincide. Thus, $\eta \approx 2e^{-1} \approx 0.736$.

With temperature-dependent thermal conductivities, similar estimations may be obtained with η becoming slightly dependent on laser power and other parameters. Correspondingly, it may be considered as a fitting parameter with $\eta \leqslant 1$.

References

1. D. Bäuerle: *Chemical Processing with Lasers*, Springer Ser. Mater. Sci. Vol. 1 (Springer, Berlin, Heidelberg 1986) D. Bäuerle: *Laser Processing and Chemistry* (Springer, Berlin, Heidelberg 1996)
2. D.J. Ehrlich, J.Y. Tsao (eds.): *Laser Microfabrication – Thin Film Processes and Lithography* (Academic, New York 1989)
3. I.W. Boyd (ed.): *Laser Surface Processing and Characterization*, EMRS Symp. Proc. **24** (North-Holland, Amsterdam 1992)
4. G. Leyendecker, D. Bäuerle, P. Geittner, H. Lydtin: Appl. Phys. Lett. **39**, 921 (1981)
   D. Bäuerle, P. Irsigler, G. Leyendecker, H. Noll, D. Wagner: Appl. Phys. Lett. **40**, 819 (1982)
5. R. Kullmer, B. Kargl, D. Bäuerle: Thin Solid Films **218**, 122 (1992)
6. M. Jubber, J.I.B. Wilson, J.L. Davidson, P.A. Fernie, P. John: Appl. Phys. Lett. **55**, 1477 (1989)
7. T.H. Baum, P.B. Comita, T.T. Codas: SPIE Proc. **1598**, 122 (1991)
8. N. Arnold, D. Bäuerle: Microelectron. Eng. **20**, 43 (1993)
9. J. Han, K.F. Jensen: J. Appl. Phys. **75**, 2240 (1994)
10. N. Arnold, P.B. Kargl, D. Bäuerle: Appl. Surf. Sci. **36**, 457 (1994)
11. D. Bäuerle, G. Leyendecker, D. Wagner, E. Bauser, Y.C. Lu: Appl. Phys. A **30**, 147 (1983)
12. P.C. Nordine, S.C. de la Veaux, F.T. Wallenberg: Appl. Phys. A **57**, 97 (1993)
13. S. Johansson, J. Schweitz, H. Westberg, M. Boman: J. Appl. Phys. **72**, 5956 (1992)
14. H. Westberg, M. Boman, S. Johansson, J. Schweitz: J. Appl. Phys. **73**, 7864 (1993)
15. H.S. Carslaw, J.C. Jaeger: *Conduction of Heat in Solids* (Oxford Univ. Press, New York 1959)
16. D. Bäuerle, B. Luk'yanchuk, K. Piglmayer: Appl. Phys. A **50**, 385 (1990)
17. J. Mathews, R.L. Walker: *Mathematical Methods of Physics* (W. Benjamin, New York 1970)
18. J. Doppelbauer: Linz (1987) Kinetische Untersuchungen an laser induzierten pyrolytischen Prozessen. Dissestation
19. J. Doppelbauer, D. Bäuerle: In *Interfaces Under Laser Irradiation*, ed. by L.D. Laude, D. Bäuerle, M. Wautelet, NATO ASI Ser. E **134**, 277 (Nijhoff, Dordrecht 1987)
20. *Gas Encyclopedia* (Elsevier, Amsterdam 1976)
21. G.G. Bentini, M. Bianconi, C. Summonte: Appl. Phys. A **45**, 821 (1988)